International Journal of Chemical Kinetics

WILEY

RESEARCH ARTICLE OPEN ACCESS

Effect of HBr on Explosion Limits of Stoichiometric Hydrogen-oxygen Mixture

Chunkan Yu[1] | Peter Glarborg[2]

[1]Institute of Technical Thermodynamics (ITT), Karlsruhe Institute of Technology (KIT), Karlsruhe, Baden-Württemberg, Germany | [2]DTU Chemical Engineering, Technical University of Denmark, Lyngby, Denmark

Correspondence: Chunkan Yu (chunkan.yu@kit.edu)

Received: 5 May 2025 | **Revised:** 25 February 2026 | **Accepted:** 16 April 2026

Keywords: auto-ignition | explosion limit | HBr inhibitor | hydrogen combustion

ABSTRACT

This work, based on numerical simulations, discusses the effect of HBr as an inhibitor on the explosion limit of stoichiometric hydrogen-oxygen gas mixture in a closed spherical vessel. The numerical simulation solves the complete governing equations for mass, momentum, species and energy. In addition, wall surface reactions are included to describe the destruction of chemically reactive radicals. The in-house *INSFLA* code is used, which takes into account the differential diffusion and thermal diffusion (Soret effect) to describe the mass transport of species within the system. The inhibitory effect of HBr on all three explosion limits under the considered conditions is analyzed based on sensitivity analysis of the explosion limit with respect to chemical reaction rates and reaction pathway analysis. It is found that the main reason for the inhibition effect is the chain-propagating step HBr+H → Br+H_2 which is in effect terminating. However, each of the three explosion limits is governed by different key reactions.

1 | Introduction

Hydrogen, being a potential zero-carbon clean fuel without emitting greenhouse gases, is applied in various engineering application. For example, hydrogen-powered vehicles are intensively developed and improved. Hydrogen internal combustion engines (H2-ICE) offer several advantages over traditional fuel engines. Besides the fact of zero carbon emissions, hydrogen engines achieve higher thermal efficiency due to its faster combustion rate [1–3]. Additionally, hydrogen engines can be adapted from existing internal combustion engine technology, making them a cost-effective transition option for manufacturers [2, 4]. In industrial manufacturing based on oxyhydrogen torch, combustion of hydrogen-oxygen mixture is further used for cutting and welding metals [5]. In the iron and steel industry, natural gas is increasing replaced by hydrogen to supply high-temperature heat in the electric arc furnace, aiming at the decarbonizing [6, 7].

Despite being a potential zero-carbon clean fuel that does not emit greenhouse gases during combustion, hydrogen presents significant safety challenges due to its highly flammable and explosive nature [8–10]. Additionally, it has a very low ignition energy, meaning even a small value of spark deposition energy can result in an explosion or a fast flame formation and propagation [10, 11]. These properties have raised significant concerns about process safety in hydrogen production, storage, transportation, and utilization within the energy industry [12–14]. Consequently, research on inhibitors to identify efficient and reliable methods for suppressing hydrogen ignition and reaction is of great interest. Inhibitors, also known as explosion suppressants or flame retardants, are substances added to a system to prevent or mitigate explosions. In the context of hydrogen, inhibitors can play a significant role in enhancing process safety and usage. For example, inhibitors can effectively narrow the flammability limits and slow down the propagation of a flame [15, 16]. In [17], ammonia serves as a combustion inhibitor to eliminate engine knock in the

direct-injection hydrogen engines at stoichiometric and wide-opening throttle conditions. A review on suppression effects of various inhibitors (up to eighty compounds) on hydrogen-air flame can be found in for example,[18], and a recent review on chemical inhibition of hydrogen-air explosions can be found in [19].

While most of these studies primarily concentrate on the suppression effect on flammability limits and laminar premixed flames, specifically in terms of laminar burning velocity, there are few investigations reporting the inhibitor effect on the explosion limit of the hydrogen/oxygen system, which can be attracting for the process safety. Unlike the flammability limits which the concentration range of a flammable gas within which flame front can be steadily propagated, the explosion limits refers to conditions where combustion occurs rapidly enough to cause an explosion (i.e., rapid temperature rise). In the present work, the hydrogen bromide (HBr) is considered as inhibitor for the hydrogen-oxygen reaction system. Although HBr is toxic and corrosive and therefore not suitable for direct use as an industrial fire suppressant, its fundamental role in bromine-based inhibition chemistry makes it an ideal model system for mechanistic investigation. Even for brominated hydrocarbons and commercial inhibitors such as CF_3Br and $C_3H_2F_3Br$ [20–22], the suppression chemistry is largely governed by the HBr subset of reactions [23]. Therefore, investigating the effect of HBr provides an a priori understanding of the inhibition mechanisms of other brominated hydrocarbon-based inhibitors. Furthermore, Dixon-Lewis et al. [23] updated and validated the Br/H/O sub-mechanism against measurements of the second explosion limit and laminar burning velocity, offering a reliable kinetic foundation for the present work. Studying HBr directly also allows the chemical effects to be isolated from the complicating chemical reaction pathways of larger halogenated species, enabling a clearer and easier mechanistic interpretation. While most existing studies focus primarily on the impact of HBr on laminar burning velocity, the present work aims to extend this understanding by examining how HBr modifies all three explosion limits of the hydrogen–oxygen system. Thus, the objective is not to propose HBr as a practical suppressant, but to use it as a canonical representative of bromine-driven inhibition chemistry relevant to a broader class of brominated inhibitors. Several important scientific questions will be addressed:

- How does the addition of HBr affect the explosion limit of the hydrogen-oxygen mixture? Does the addition of HBr suppress the explosion of hydrogen-oxygen mixtures, which is similar to its effect on laminar flame speed and flammability limit?
- If HBr has a suppressive effect on the explosion limit of a hydrogen-oxygen mixture, do the controlling chemical reactions that correspond to different explosion limits remain the same, or do different explosion limits have different key reactions that lead to the explosion?
- The presence of HBr can introduce additional surface reactions involving atomic Br radical. Would these surface reactions have an impact on the explosion limits?

This work is organized as follows: First, the mathematical modeling of the auto-ignition process for studying the explosion limit will be introduced. The applied chemical mechanism will then be validated against experimental measurements from the literature. Next, the explosion limit in the presence of HBr will be presented, together with a brief discussion on the definition of a successful explosion. Different explosion limits will then be investigated through sensitivity analysis of the explosion temperature with respect to the chemical reaction rate and reaction pathway analysis of selected species. Here throughout the whole work the explosion temperature is defined as the minimum mixture temperature at which an explosion can occur. Finally, the conclusions will be summarized, and some perspectives for further research will be suggested.

2 | Mathematical Model

To determine the explosion limit, the auto-ignition process is modeled in a spherical closed vessel with one-dimensional geometry. Corresponding to the experimental setup in [24–26], the gas mixture inside the reactor is spatially homogeneously distributed and initially at a high temperature, such that the mixture undergoes spontaneous explosion without the need for any external energy source, such as spark ignition. While a detailed discussion and derivation of the mathematical formulation for the governing equations of species mass, momentum, and energy can be found in [27], this section will provide a brief overview of governing equations, chemical mechanism and numerical software applied in the present work for better clarity. More details can be found in the corresponding provided references.

It should be emphasized that a spatially resolved 1D model in the present work is more suitable for determining explosion limits compared to the 0D homogeneous auto-ignition reactor used in for example, [28–30]. A 0D homogeneous auto-ignition reactor requires an artificial explosion definition (e.g., specifying a temperature-rise threshold [28, 29] or consumption threshold of fuels [30]), and the predicted limits are sensitive to such user-defined criteria. In contrast, as will be shown later, in the absence of an explosion the temperature and species profiles remain flat in both space and time, whereas an explosion is characterized by a sharp rise in temperature or main products. This makes the 1D model a more objective and physically tool for identifying explosion behavior.

2.1 | Governing Equations

According to [27], the governing equations are formulated by using the Lagrangian coordinate $\psi(r,t) = \int_0^r \rho(r,t) r^\alpha \mathrm{d}r$ [31], in which r is the radius, t the time and ρ the density. Furthermore, $\alpha = 1$ is for cylinder and $\alpha = 2$ for sphere. By introducing the Lagrangian coordinate, the convection terms from the governing equations are eliminated, and the continuity equation becomes unnecessary in Lagrangian coordinates, as it is automatically satisfied following the transformation [27, 32]. Consequently, the governing equation simplified to [27, 33]:

$$\frac{\partial r}{\partial \psi} - \frac{1}{\rho r^\alpha} = 0 \tag{1}$$

$$\frac{\partial p}{\partial \psi} = 0 \tag{2}$$

$$\frac{\partial w_i}{\partial t} + \frac{\partial}{\partial \psi}(\rho r^{\alpha} w_i V_i) - \frac{\dot{\omega}_i M_i}{\rho} = 0 \tag{3}$$

$$\frac{\partial T}{\partial t} - \frac{1}{\rho c_p}\frac{\partial p}{\partial t} - \frac{1}{c_p}\frac{\partial}{\partial \psi}\left(\rho r^{2\alpha}\lambda \frac{\partial T}{\partial \psi}\right) + \frac{r^{\alpha}}{c_p}\sum_{i=1}^{n_s}\rho w_i V_i c_{pi}\frac{\partial T}{\partial \psi} + \frac{1}{\rho c_p}\sum_{i=1}^{n_s}\dot{\omega}_i h_i M_i = 0 \tag{4}$$

where t and ψ are two independent variables, and all other thermo-kinetic quantities and physical variables are functions of t and ψ: $r = r(t,\psi)$, $T = T(t,\psi)$, $p = p(t,\psi)$, and $w_i = w_i(t,\psi)$. In these equations, p = pressure, T = temperature, c_p = isobaric specific heat capacity of the mixture, λ = heat conductivity of the mixture, n_s = number of species, w_i = mass fractions of species i, M_i = molar mass of species i, h_i = specific enthalpy of species i, $\dot{\omega}_i$ = molar formation rate of species i, c_{pi} = isobaric heat capacity of species i. V_i represents the diffusion velocity of species i, including the differential diffusion and thermal diffusion (Soret effect).

This mathematical model solves the governing partial differential equations by incorporating molecular transport processes, such as heat conduction and molecular diffusion. These transport mechanisms play significant role in accurately capturing the explosion limits, since species can diffuse towards the wall surface and undergo surface reactions.

2.2 | Reaction at the Wall Surface

As reported in various literature [27, 34–36], reactions at the vessel surface play a crucial role in the auto-ignition process within a closed vessel. These surface reactions include phenomena such as surface recombination of atoms or surface destruction of reactive molecules. For the hydrogen-oxygen system, we adopt the simple surface reaction model described in [27], which includes five recombination/destruction reactions of reactive molecules on the surface, together with one additional surface reaction involving the destruction of chemically reactive atomic Br at the wall surface, as follows:

$$\text{(S1)}\ \mathrm{HO_2} \xrightarrow{\text{wall}} \frac{1}{2}\mathrm{H_2O} + \frac{3}{4}\mathrm{O_2}$$

$$\text{(S2)}\ \mathrm{O} \xrightarrow{\text{wall}} \frac{1}{2}\mathrm{O_2}$$

$$\text{(S3)}\ \mathrm{H} \xrightarrow{\text{wall}} \frac{1}{2}\mathrm{H_2}$$

$$\text{(S4)}\ \mathrm{OH} \xrightarrow{\text{wall}} \frac{1}{2}\mathrm{H_2O} + \frac{1}{4}\mathrm{O_2}$$

$$\text{(S5)}\ \mathrm{H_2O_2} \xrightarrow{\text{wall}} \mathrm{H_2O} + \frac{1}{2}\mathrm{O_2}$$

$$\text{(S6)}\ \mathrm{Br} \xrightarrow{\text{wall}} \frac{1}{2}\mathrm{Br_2}$$

The mass rate of formation per unit surface area due to the surface reaction $\dot{\omega}_k^s$ is quantified by the surface destruction efficiency γ_k, where index k stands for the species k. A higher value of γ_k indicates a faster destruction of radicals at the wall surface. A more detailed modeling for surface reaction including the determination of mass rate of formation per surface unit and surface collision number of one species can be found in [27, 37]. A surface destruction efficiency of $\gamma = 1 \cdot 10^{-3}$ is suggested to all surface reactions, because this choice has been shown to provide reasonable predictions for all explosion limits of stoichiometric hydrogen-oxygen mixtures, as illustrated in [27].

2.3 | Boundary Conditions

To ensure computational efficiency, the simulation domain is defined from the reactor center to the wall surface. At the center of the reaction vessel ($\psi = 0$), symmetry boundary conditions are applied:

$$r(\psi = 0, t) = 0, \quad \left.\frac{\partial T}{\partial \psi}\right|_{\psi=0,t} = 0, \quad \left.\frac{\partial w_i}{\partial \psi}\right|_{\psi=0,t} = 0. \tag{5}$$

At the outer boundary condition (applied at the vessel surface ($\psi = \psi^s$)), the temperature is assumed to be constant at T_0, and the total mass flux of species i vanishes at the surface. Thus the corresponding boundary conditions are formulated as:

$$r(\psi = \psi^s, t) = R, \quad T(\psi = \psi^s, t) = T_0, \quad \rho w_i V_i + \dot{\omega}_i^s = 0, \tag{6}$$

where R is the radius of the vessel. We notice that at the wall surface, the temperature is set to a fixed value. This is because the thermal transmittance of the solid wall is much higher than that of the gas phase, allowing us to assume a negligible temperature gradient within the solid wall. Furthermore, when a temperature gradient exists in the gas near the wall surface, heat loss from the gas to the wall is also taken into account. Later, we will show through comparison with measurements that this choice of temperature boundary condition is reasonable.

2.4 | Software: In-House INSFLA Code

In this study, numerical simulations are conducted using the in-house code INSFLA [27]. The spatio-temporal evolution of the underlying system of partial differential equations (PDEs) is solved using the method of lines, with given initial and boundary conditions. The integration time step is automatically adapted based on error control. Additionally, an algorithm for automatic adaptive mesh grid is employed to ensure that grid points are sufficient in regions with high scalar gradients, while fewer grid points are distributed in regions with small scalar gradients. This approach optimizes computational efficiency while maintaining high accuracy. The INSFLA code has been widely validated against experiment measurement for various combustion scenarios such as three explosion limits for auto-ignition process [27], laminar burning velocity for laminar premixed flame [38], extinction strain rate for counterflow diffusion flames [39] and others.

2.5 | Gas Mixture and Chemical Mechanism

The combustible mixture consists mainly of stoichiometric hydrogen/oxygen (H_2:O_2 = 2:1), with additional HBr doped into.

TABLE 1 | Selected important chemical reaction steps in the H_2/O_2/HBr reaction, and their rate coefficients. The rate constants are expressed in terms of a modified Arrhenius as $k = AT^n \exp(-E_a/(RT))$. Units are kJ, cm, mole, s. Detailed sub-mechanism for H/O is from [27], and sub-mechanism for Br/H/O is from [23].

	Elementary reactions	A	n	E_a	Ref.
(R1)	$H + O_2 \rightleftharpoons OH + O$	2.00×10^{14}	0.00	70.3	[27]
(R8)	$H + O_2 + M \rightleftharpoons HO_2 + M$[a]	2.30×10^{18}	−0.80	0.00	[27]
(R9)	$HO_2 + H \rightleftharpoons OH + OH$	1.50×10^{14}	0.00	4.20	[27]
(R14)	$HO_2 + HO_2 \rightleftharpoons H_2O_2 + O_2$	2.50×10^{11}	0.00	−5.20	[27]
(R16)	$H_2O_2 + H \rightleftharpoons H_2 + HO_2$	1.70×10^{12}	0.00	15.70	[27]
(R20)	$H + Br + M \rightleftharpoons HBr + M$[b]	1.90×10^{21}	−1.87	0.00	[23]
(R21)	$HBr + H \rightleftharpoons H_2 + Br$	1.30×10^{10}	1.05	0.682	[23]
(R24)	$HBr + HO_2 \rightleftharpoons Br + H_2O_2$	4.20×10^{2}	2.93	32.123	[23]
(R26)	$Br + HO_2 \rightleftharpoons HBr + O_2$	8.60×10^{9}	1.00	1.96	[23]
(R27)	$Br + Br + M \rightleftharpoons Br_2 + M$[c]	1.50×10^{14}	0.00	−7.118	[23]
(R34)	$BrO + OH \rightleftharpoons Br + HO_2$	1.10×10^{13}	0.00	−2.081	[23]

aThird body efficiencies: $H_2 = 1.0$, $O_2 = 0.35$, $H_2O = 6.5$.
bThird body efficiencies: HBr = 2.7, $H_2O = 5.0$.
cThird body efficiencies: $H_2O = 5.4$, $Br_2 = 0.0$.

The amount of added HBr is expressed by the HBr mole fraction in the unburnt gas mixture as

$$X(\mathrm{HBr}) = \frac{n(\mathrm{HBr})}{n(\mathrm{H_2}) + n(\mathrm{O_2}) + n(\mathrm{HBr})} \tag{7}$$

where n_i is the molar amount of component i in the mixture.

The corresponding chemical kinetics comprises two sub-mechanisms. The H_2/O_2 sub-mechanism is adopted from [27], exhibiting high accuracy in predicting all explosion limits compared to experimental measurements. The Br/H/O subset of the reaction mechanism is sourced from [23]. In Table 1, several important reaction steps necessary for the discussion are listed with the corresponding rate constants.

It should be emphasized that experimental data for HBr-containing H_2/O_2 systems are limited to ppm-level HBr concentrations in [23]. As a result, the present chemical mechanism cannot be fully validated across the entire parameter space studied here. The results based on this mechanism should therefore be interpreted primarily as providing qualitative mechanistic insight into bromine-driven inhibition, rather than as quantitatively exact predictions. Additional experimental measurements at higher HBr concentrations and over wider pressure ranges would be highly valuable for further constraining and improving the kinetic mechanism.

Additionally, it is noted that in [23], no information regarding Br species is provided. Therefore, the Lennard–Jones parameters and related transport coefficients for Br species used in the present study was taken from Noto et al. [40].

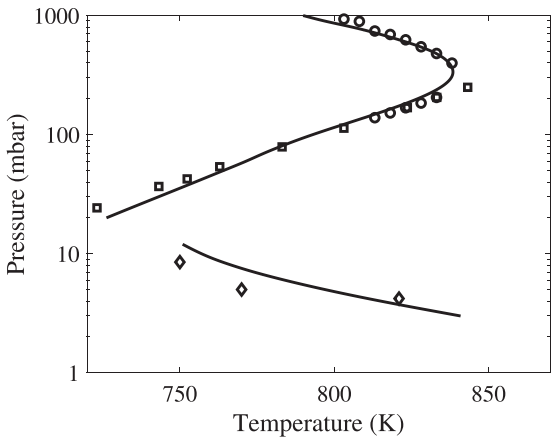

FIGURE 1 | Computed and experimental explosion limits for stoichiometric H_2-O_2 mixtures. Symbols for measurements: black diamonds from [41]; black circles from [25]; black squares from [24].

2.6 | Validation of the Mathematical Models

Before discussing the major topic of the present work, it is necessary to validate both the mathematical model and the applied chemical mechanism. In Figure 1, the computed explosion limits for stoichiometric hydrogen-oxygen mixtures are compared with measurements. For these measurements, the black diamond symbols denote the first explosion limit in a cylindrical reaction vessel with a diameter of 1.8 cm, taken from [41]; the black square and circle symbols represent the second and third explosion limits in a spherical reaction vessel with a diameter of 7.4 cm, from [24, 25]. It should be emphasized that this comparison for stoichiometric hydrogen-oxygen mixtures has already been reported in [27]. Nevertheless, we present this comparison again here to allow readers to clearly and directly

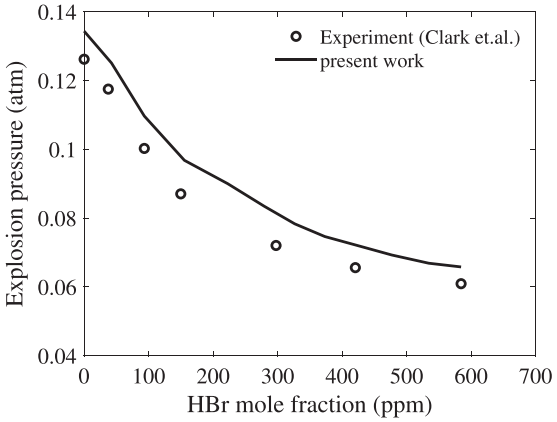

FIGURE 2 | Comparison of explosion pressure between measurements (circles) [23, 26] and predictions based on numerical simulation (solid line) using the mechanism from Table 1(lines) on the second explosion limit in a reactor at 773 K. The mixture consists of 28% H_2, 14% O_2 (H_2:O_2 = 2:1), different HBr mole fraction. The rest is N_2.

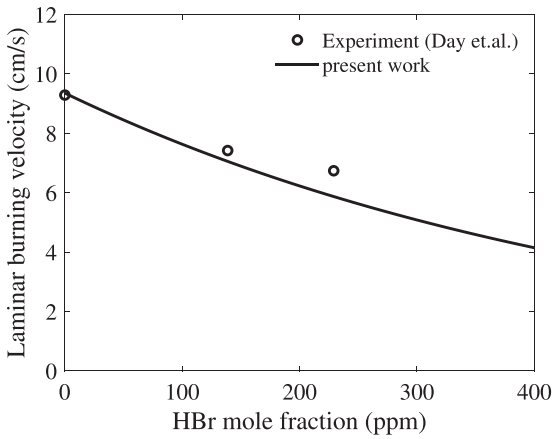

FIGURE 3 | Measured (symbols) and computed (solid line) laminar burning velocity versus HBr in mole fraction (ppm). Measurements from Day et al. [42]. Inlet gas composition was 18.8% H_2, 4.6%O_2, and 76.6%N_2 by mole, with varying amounts of HBr. The temperature of unburnt gas mixture is 336 K.

see that the mathematical model used in the present work is feasible and reliable. As shown, the computed explosion limits match the experimental results very well, indicating that the applied boundary conditions and the chosen surface destruction efficiencies $\gamma_k = 1 \cdot 10^{-3}$ are reasonable and trustworthy. Further discussion on the mathematical model can be found in [27].

Next, it is necessary to validate the chemical mechanism shown in Table 1. To this end, two different validation cases have been performed. The first validation case concerns the explosion pressure at the second explosion limit in a reactor at 773 K, as presented in Figure 2. The second validation case investigates the laminar burning velocity, as shown in Figure 3. In both cases, the numerical predictions show good agreement with the measurements, confirming the reliability of the chemical kinetic model. Such accurate numerical prediction indicates that the chemical mechanism not only captures the overall reactivity of the system but also adequately reflects the effects of HBr inhibition. The validated mechanism can thus be further applied in subsequent simulations and analyses under various operating conditions.

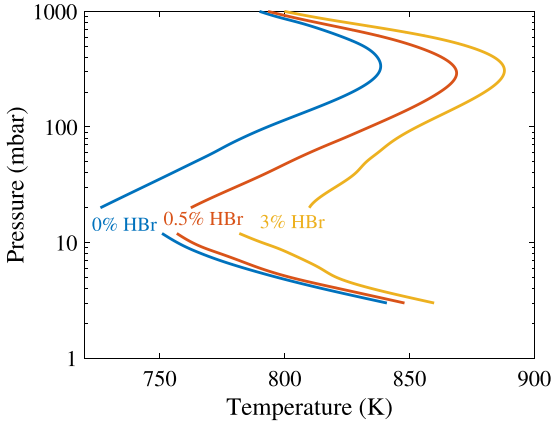

FIGURE 4 | Calculated explosion limits for 2:1 hydrogen–oxygen mixtures with different HBr addition.

3 | Results and Discussion

In the following, numerical simulations are performed to investigate the inhibitory effect of HBr on the stoichiometric hydrogen–oxygen system. The reactor geometries are chosen to be consistent with those used in the classical experimental studies reproduced in [27]: for the first explosion limit, a closed cylindrical vessel with a diameter of 1.8 cm is used [41], whereas a closed spherical vessel with a diameter of 7.4 cm is used for the second and third explosion limits [24, 25]. These specific geometries correspond directly to the vessels in which the historical explosion-limit measurements were performed, and they are the configurations for which the present mathematical model together with its boundary conditions and surface-reaction parameters (surface destruction efficiency $\gamma_k = 1 \cdot 10^{-3}$) has been validated, as shown in Figure 1. Because domain size, geometry, diffusion length scales and wall reactions strongly influence radical concentrations, adopting the same domain sizes as the validated baseline H_2/O_2 system ensures that the underlying model remains quantitatively accurate for the reference case. The use of different domain sizes is therefore not arbitrary, but rather the choice to ensure consistency with the established validation framework.

Figure 4 illustrates the calculated pressure and temperature for the explosion limits in stoichiometric hydrogen-oxygen mixtures with varying HBr mole fractions. It can be clearly observed that HBr shows an inhibitory effect, suppressing the explosion for all three explosion limits. It should be pointed out explicitly that there is a discontinuity in the curves between the first and the second explosion limits, which is only due to the use of different vessel diameters.

In the following, the effect of HBr on each explosion limit will be discussed separately. Sensitivity analysis and reaction pathway analysis of a selected species will be used to better understand the role of HBr. The sensitivity analysis is performed by increasing the rate coefficient of all elementary reactions and their reverse reactions by a factor of two. We focus on the sensitivity of the explosion temperature with respect to the reaction rate. A positive

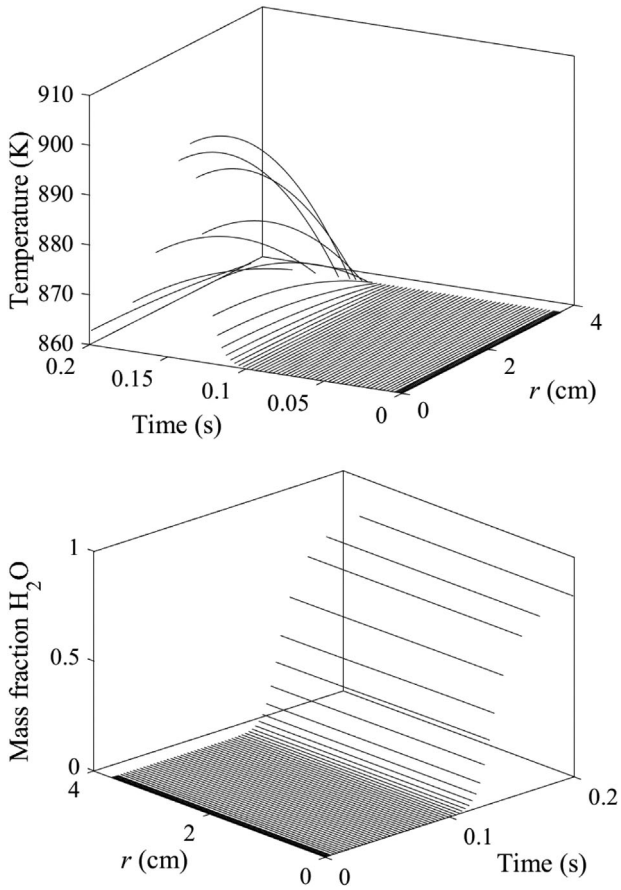

FIGURE 5 | Calculated transient profiles for temperature and mass fraction of H_2O in an igniting stoichiometric hydrogen-oxygen mixture: $p = 3$ mbar, $T = 860$ K.

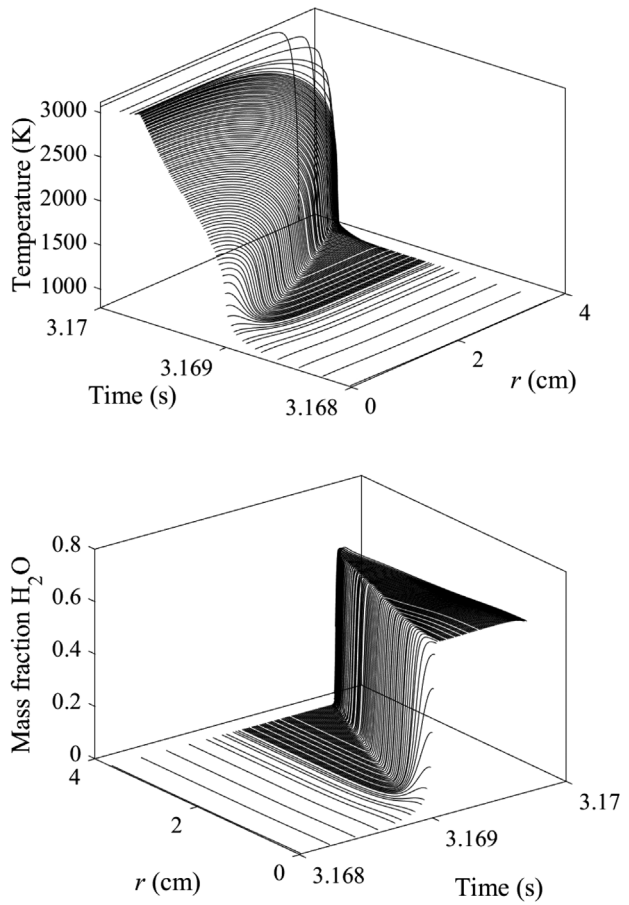

FIGURE 6 | Calculated transient profiles for temperature and mass fraction of H_2O in an igniting stoichiometric hydrogen–oxygen mixture: $p = 100$ mbar, $T = 793$ K.

sensitivity value indicates that an increase in a specific reaction rate suppresses the explosion, requiring a higher explosion temperature to initiate the process. In contrast, a negative sensitivity value indicates that the reaction promotes the explosion, leading to a lower explosion temperature.

3.1 | Transient Explosion Process and Criteria for Explosion

Before discussing the effect of HBr on various explosion limits, it is instructing to provide typical examples of a simulation of an igniting mixture for different explosion limits. Such a discussion helps us to clearly understand how the auto-ignition process is identified as a successful explosion.

Figure 5 shows typical profiles of temperature and mass fraction of H_2O for a successful auto-ignition at an initial temperature of 860 K and an initial pressure of 3 mbar, which is located in the first explosion limit. We observe in the temperature profile that the temperature at the vessel center increases only slightly after a certain induction time (around 0.1 s) from 860 K to 900 K. After the temperature increases over the whole reactor vessel, heat transfer across the reactor vessel surface leads to a decrease in temperature so that the temperature inside the reactor vessel is uniform in space and equals the surface temperature at the end. Despite a small temperature increase here, the profile of H_2O mass fraction shows that after the induction time (around 0.1 s), H_2O is produced rapidly. At around 0.2 s, although the temperature is maximally 862 K inside the vessel, the mass fraction of H_2O reaches around 0.9, indicating nearly complete reaction.

Figure 6 shows another typical profile of temperature and mass fraction of H_2O for a successful auto-ignition at an initial temperature of 793 K and an initial pressure of 100 mbar, which is located in the second explosion limit. We observe in the temperature profile that after a certain induction period (around 3.168 s in this figure), there is an extreme sharp temperature increase of approximately 3000 K at the vessel center within only a few milliseconds (around 2 ms in this figure). After ignition occurs throughout the entire reactor vessel (here after 3.17 s), heat transfer across the reactor vessel surface causes the temperature to decrease until it becomes spatially uniform and equal to the surface temperature (not shown in the Figure). Similarly, after the induction time, there is a rapid increase in H_2O mass fraction, starting in the vessel center first where high temperature is observed. At the end of ignition, the H_2O concentration approaches to the equilibrium concentration. It should be mentioned here that similar time- and spatial-dependent profiles of temperature and H_2O mass fraction can be observed for the third explosion limit, which is not shown here.

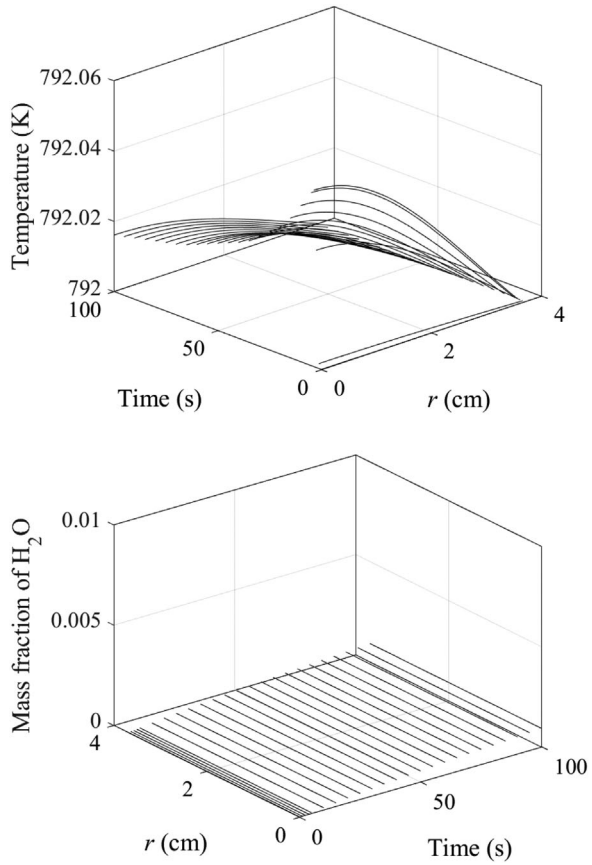

FIGURE 7 | Calculated transient profiles for temperature and mass fraction of H_2O in a failed-igniting stoichiometric hydrogen-oxygen mixture: $p = 100$ mbar, $T = 792$ K.

To better illustrate that an explosion is characterized by a sharp rise in temperature or in the mass fraction of H_2O whereas in a non-exploding case the system remains essentially unchanged, Figure 7 shows a representative example of a non-igniting condition. Here, compared with the igniting case in Figure 6, the initial temperature is reduced by only 1 K. Despite this small change, the system indicates fundamentally different behavior: the maximum temperature increase over 100 s is less than 0.04 K, and the H_2O mass fraction remains below 10^{-3}, indicating negligible reaction progress. Thus, ignition can be easily identified by examining whether a sharp increase occurs in either temperature or H_2O concentration. This clear qualitative difference enables the explosion limits to be determined without relying on any threshold-based ignition criterion, such as those used in [28–30].

To summarize, the identification of the first explosion limit requires a rapid increase in the main product (in this case, H_2O). To identify the second and third explosion limits, a rapid increase in temperature is considered as an indicator.

3.2 | First Explosion Limit

Figure 4 shows that for the first explosion limit, the addition of more HBr to the hydrogen-oxygen mixture requires a higher temperature for the onset of explosion. This indicates the inhibition effect of HBr on the explosion behavior. In order to find

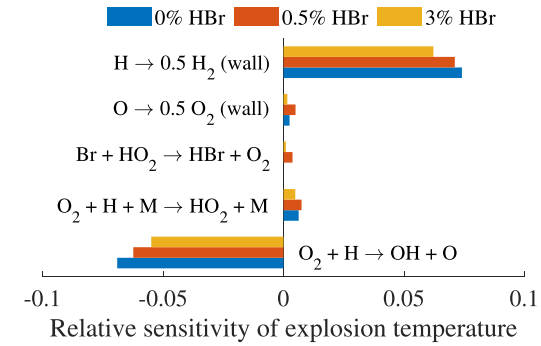

FIGURE 8 | Relative sensitivity explosion temperature at first explosion limit for different HBr addition in a stoichiometric H_2-O_2 mixture at $p = 5$mbar and the time point of the maximum temperature increase $(\max\left(\frac{dT}{dt}\right))$.

out the dominant elementary reactions contributing to the first explosion limit, a sensitivity analysis for different HBr addition is performed and represented in Figure 8 at $p = 5$mbar, showing the most sensitive elementary reactions. The elementary reactions, which are not shown in the figure, have then minor or almost no effect on the second explosion limit. It is observed that even with the presence of HBr, the most sensitive reactions are still mainly related to the consumption of H radicals based on the chain branching reaction (R1) and chain termination reaction (S3)

$$\text{(R1)} \quad \mathrm{H + O_2 \rightarrow\ OH + O}$$

$$\text{(S3)} \quad \mathrm{H \xrightarrow{wall} \frac{1}{2}H_2}$$

Addition of HBr leads to another chain termination through reaction (R26) $Br+HO_2 \rightarrow HBr+O_2$ in Figure 8, which on the other hand still has small sensitivity value. It is interesting to note that the inclusion of surface reactions involving the destruction of atomic Br (e.g., surface reaction S6) has almost no observable impact on this explosion limit, and thus no sensitive behavior. This can be attributed to the relatively low concentration of atomic Br generated from the added HBr, which remains significantly lower than that of highly reactive radicals such as H radicals. Even with an HBr concentration as high as 3%, the amount of atomic Br is insufficient to contribute meaningfully to radical loss at the reactor wall surface. As a result, the overall influence of atomic Br destruction at the wall surface becomes negligibly small.

In order to support the sensitivity analysis and understand the suppression effect of HBr on the explosion temperature, Figure 9 shows the main consumption of H radicals for the non-explosion case (left) and the explosion case (right) at $p = 5$ mbar. For the explosion case, 0.5% HBr addition (percentage in []) and 3% HBr addition (percentage in ()) at explosion limits are considered. Two major observations can be addressed here:

- For the non-explosion case, a large amount of H radicals is consumed at the wall surface to form stable H_2. On the other hand, for the explosion case, the H radicals are only consumed in a small amount at the wall surface. The majority of H

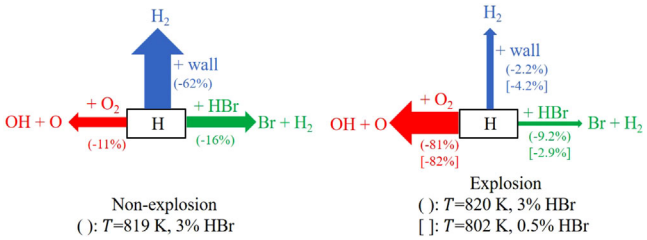

FIGURE 9 | Main consumption of H radical for non-explosion case (left) and explosion case with two different HBr addition (right). All cases at $p = 5$ mbar and the time point of the maximum temperature increase (max $\left(\frac{dT}{dt}\right)$).

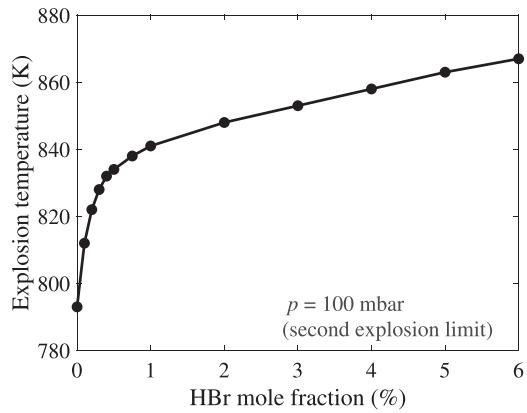

FIGURE 10 | Explosion temperature versus HBr mole fraction at p = 100 mbar, which is at second explosion limit.

radicals is consumed through the chain branching reaction (R1) H+O_2 → OH+O, leading to mixture explosion.

- However, in the presence of HBr, a portion of the H radicals will be consumed through the reaction step

$$\text{(R21)} \quad \text{HBr} + \text{H} \rightarrow \text{Br} + \text{H}_2.$$

It should be explicitly emphasized that although atomic Br is also a highly reactive species, it is less reactive than H radicals. Therefore (R21) is a chain propagation reaction that is in effect terminating, which serves to slow down the growth of radical-pool population. This explains the inhibitory effect of HBr at the first explosion limit, where the addition of HBr leads to a higher required explosion temperature.

3.3 | Second Explosion Limit

In this part, we focus to the second explosion limit. Figure 4 shows that also for the second explosion limit, HBr acts as an inhibitor for the H_2/O_2 system, as a higher temperature is required to initiate an explosion. Figure 10 illustrates the relationship between the explosion temperature and the HBr mole fraction. In this figure, we have selected 100 mbar as a representative candidate for the second explosion limit. We can clearly observe that as the HBr mole fraction increases, the explosion temperature rises in a monotonic manner. In the following, we will further study the second explosion limit in detail.

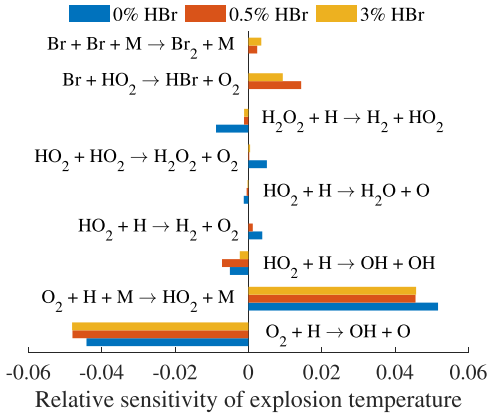

FIGURE 11 | Relative sensitivity explosion temperature at second explosion limit for different HBr addition in a stoichiometric H_2-O_2 mixture at $p = 100$mbar and the time point of the maximum temperature increase (max $\left(\frac{dT}{dt}\right)$).

Figure 11 shows the most sensitive elementary reactions to the second explosion temperature at p = 100mbar. Consistent with explanations found in literature [24, 33, 34, 43] for the H_2/O_2 explosion system, regardless of the HBr addition the second explosion limit is primarily influenced by the competition between the chain branching reaction (R1) and the chain termination reaction (R8)

$$\text{(R1)} \quad \text{H} + \text{O}_2 \rightarrow \text{OH} + \text{O}$$

$$\text{(R8)} \quad \text{H} + \text{O}_2 + \text{M} \rightarrow \text{HO}_2 + \text{M}$$

Several elementary reactions involving HO_2, such as (R14) $HO_2 + HO_2 \rightarrow H_2O_2 + O_2$ and (R16) $H_2O_2 + H \rightarrow H_2 + HO_2$, which are sensitive in the H_2/O_2 mixture, become noticeably less important with the addition of HBr. In the presence of HBr, the HO_2 radical participates in a chain termination reaction

$$\text{(R26)} \quad \text{Br} + \text{HO}_2 \rightarrow \text{HBr} + \text{O}_2,$$

which shows the third most sensitive elementary reactions. Furthermore, Br+Br+M → Br_2+M (R27) serves as another chain termination step, but with small sensitivity values.

The inhibitory effect of HBr on the second explosion limit can be further understood by investigating the reaction pathway analysis. From the sensitivity analysis (c.f. Figure 11), it can be concluded that the consumption of H radical and atomic Br plays a significant role in the second explosion limit. Therefore, in Figure 12, the main sources of consumption for H radical and atomic Br are shown.

Starting with the non-explosion case, the following two major observation must be mentioned:

- With the presence of HBr, H radicals are predominantly consumed through the chain termination three-body reaction (R8) H+O_2+M → HO_2+M, producing the mildly reactive hydroperoxyl radicals (HO_2) and preventing explosion. It is interesting to note that the second major consumption of H radicals is the chain propagating step (R21) HBr+H → Br+H_2

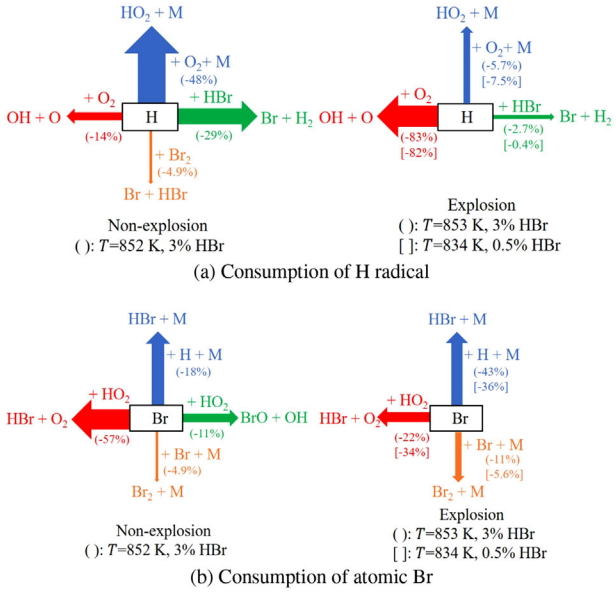

FIGURE 12 | Main consumption of H radical (upper) and atomic Br (lower) for non-explosion case (left) and explosion case with two different HBr addition (right). All cases at $p = 100$ mbar and the time point of the maximum temperature increase (max $\left(\frac{dT}{dt}\right)$).

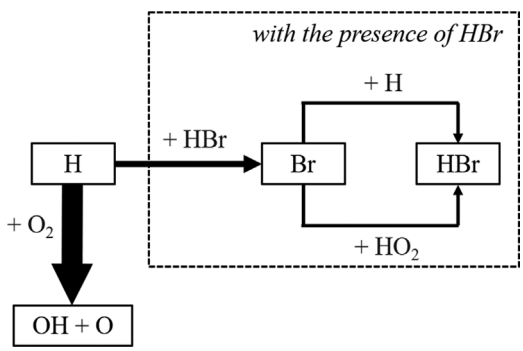

FIGURE 13 | Reaction pathway for the illustration of HBr inhibition effect at the second explosion limit.

which is in effect terminating which produces a large amount of atomic Br.

- Although a large amount of atomic Br is produced, it is mainly consumed via another two chain termination steps (R20) and (R26). The third-body reaction H+Br+M → HBr+M (R20) consumes directly active H radicals. The reaction (R26) Br+HO_2 → HBr+O_2 involves the participant of HO_2, which is produced via another chain termination reaction (R8). Therefore, although atomic Br is produced, it will be consumed again to produce stable HBr and O_2 molecules.

We now focus on cases where the explosion is successful. To explain the phenomenon where increasing HBr suppresses H_2/O_2 explosion at second explosion limit, we will analyze main consumption of H radical and atomic Br in Figure 12 (right column), together with Figure 13. Here Figure 13 represents the simplified reaction pathway for the illustration of HBr inhibition effect at the second explosion limit derived from the observation shown in Figure 12 (right column). It can be observed that

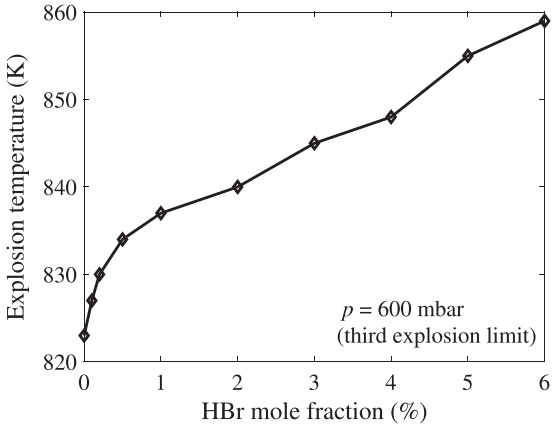

FIGURE 14 | Explosion temperature versus HBr mole fraction at $p =$ 600 mbar, which is both at third explosion limit.

regardless of whether HBr is present or not, the radicals increase at an exponential rate, mostly via the chain branching step (R1) H+O_2 → O+OH, whose rate is far faster than other reactions such as chain termination reaction (R8) H+O_2+M → HO_2+M and chain propagating reaction which is in effect terminating (R21) HBr+H → Br+H_2. With the presence of HBr, some amount of H radicals will react with HBr, producing the less reactive atomic Br via (R21) HBr+H → Br+H_2, which is then consumed again to produce HBr. Throughout this process, the presence of HBr slows down the production rate of reactive radicals, thereby achieving the inhibitory effect.

3.4 | Third Explosion Limit

In this last section, we will discuss the third explosion limit. Figure 14 presents the curve of explosion temperature as a function of HBr mole fraction in H_2/O_2 mixture. Here, 600 mbar is chosen as a representative example. Similar to the other two explosion limits, in the third explosion limit, an increase in HBr concentration suppresses the hydrogen-oxygen explosion. As a result, achieving an explosion requires a higher explosion temperature. Same as the other two explosion limits, with the presence of HBr, the reaction step (R21) HBr+H → Br+H_2 serves to inhibit reaction, slowing down the production rate of H radicals and thereby achieving the inhibitory effect. However, as will be shown below, the effect of HBr at the third explosion limit differs from that at other explosion limits, and the key controlling reactions are worth investigating.

In order to investigate the effect of HBr at the third explosion limit, sensitivity analysis is performed to find out the most sensitive reactions, as shown in Figure 15 at $p = 600$ mbar as representative example. When we compare with the sensitivity of the second explosion limit (c.f. Figure 11), we find that more chemical reactions involving HO_2 become more sensitive, turning into a more crucial reaction step in the process. Among them are for example, (R24) HBr+HO_2 → Br+H_2O_2 and (R34) BrO+OH → Br+HO_2. Additionally, we observe that the destruction of HO_2 radicals at the wall surface becomes noticeable for pure H_2-O_2 system, but its sensitivity values remain small in the presence of HBr. Therefore, the discussion on the sensitivity analysis

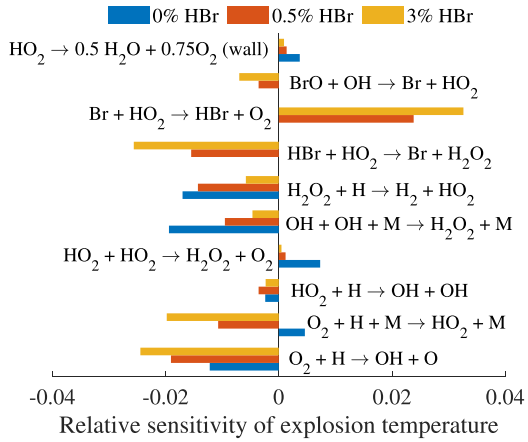

FIGURE 15 | Relative sensitivity explosion temperature at third explosion limit for different HBr addition in a stoichiometric H_2-O_2 mixture at $p = 600$ mbar and the time point of the maximum temperature increase (max $\left(\frac{dT}{dt}\right)$).

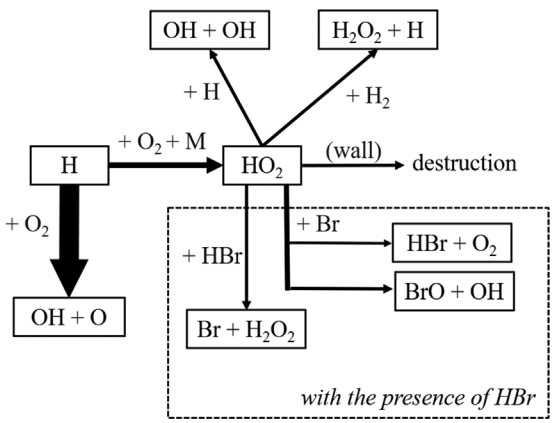

FIGURE 16 | Reaction pathway for the illustration of HBr inhibition effect at the third explosion limit.

will be conducted together with Figure 16, allowing us to better understand how key reaction steps influence the third explosion limit.

It is straightforward that the chain termination step (R8) $H+O_2+M \rightarrow HO_2+M$ is still important at the high pressure. For pure hydrogen-oxygen mixtures, the sensitivity of this reaction is still positive but greatly reduced compared to the second explosion limit. According to the reaction pathway shown in Figure 16, under these relatively high-pressure conditions, the HO_2 generated through the chain termination step (R8) will be further consumed through the chain branching step (R9) $HO_2+H \rightarrow OH+OH$. Additionally, HO_2 also opens up the H_2O_2 chain sequence through the chain propagation step (R16) $HO_2+H_2 \rightarrow H_2O_2+H$. Although the production of HO_2 would benefit other chain-branching steps that promote ignition at high pressures, the termination of the HO_2 radical at the wall surface suppresses its production and thus serves to slow down the reaction. Therefore, the sensitivity value of the wall destruction reaction of HO_2 is positive. These results are consistent with the conclusions reported in for example, [33, 35, 44].

It is noteworthy that, in the presence of HBr, the sensitivity of the chain termination step (R8) becomes negative, which implies that this reaction (R8) would actually promote an explosion. By integrating sensitivity analysis from Figure 15 with the reaction pathway from Figure 16, we can observe that with the presence of HBr, the consumption of HO_2 follows some new reaction channels:

- One reaction pathway is (R24) $HO_2+HBr \rightarrow H_2O_2+Br$. Since Br is highly reactive compared to HO_2, this serves as a chain-propagating step, effectively promoting the reaction. Furthermore, this step also benefits the production of H_2O_2, which initiates its chain sequence for further chain propagation and chain branching steps [35, 44]. Therefore, (R24) also has a positive sensitivity value. However, the production of atomic Br due to HO_2 via (R24) is slower than the production of H radical due to HO_2 via (R16) $HO_2+H_2 \rightarrow H_2O_2+H$. Thus, the presence of HBr slows down this chain propagating step which effectively promotes the reaction, and thus serves as inhibitory effect.
- The other reaction pathway involves the consumption of HO_2 through its reaction with atomic Br. The step (R26) $HO_2+Br \rightarrow O_2+HBr$ is a chain-termination step, which therefore has a positive sensitivity value. In contrast, the step (R34) $HO_2+Br \rightarrow BrO+OH$ is a chain propagating step which is in effect promoting, since the OH radical is much more chemically reactive than atomic Br. This also explains why (R34) has a negative sensitivity value. Reaction pathway analysis shows that (R34) consumes more HO_2 through its reaction with Br than (R24). Therefore, overall, the reaction steps involving HO_2+Br promote the explosion. However, these reaction steps are still slower than the reaction step (R9) $HO_2+H \rightarrow OH+OH$. Therefore, the presence of atomic Br continues to show an inhibitory effect.

It is interesting to observe that the wall destruction of HO_2 almost loses its significance in the presence of HBr. This is mainly because more HO_2 radicals participate in gas-phase reactions with Br-containing species, reducing the number of HO_2 radicals that can diffuse towards the wall surface and are destroyed there. As a result, the influence of surface reactions involving HO_2 reduces at third explosion limit. This shift shows the competitive nature between gas-phase reactions and HO_2 surface reaction in determining HO_2 radical concentrations under the influence of HBr added into the hydrogen-oxygen mixture.

To summarize, in the presence of HBr, the produced HO_2 can further participate in additional chain-propagating steps, effectively promoting the reaction. Consequently, the overall sensitivity of (R8) becomes negative, indicating its promoting effect on the explosion.

3.5 | Practical Impact

From a practical perspective, the present results provide mechanistic guidance for understanding and modeling explosion suppression in hydrogen systems. The present work shows that explosion limits are controlled by different dominant reactions at different pressure regimes, and that inhibitors such as HBr

interact with these regimes in different manners. This insight is particularly relevant for safety-oriented modeling of hydrogen storage, handling, and processing systems, where explosion limits, rather than steady flames, are often the governing concern. Moreover, the limit-specific reaction pathways identified here may serve as a useful reference for the development or assessment of alternative bromine-containing or halogen-based inhibitors in future studies.

4 | Conclusion

The auto-ignition process of stoichiometric hydrogen-oxygen gas mixtures has been modeled in a spherical closed vessel. HBr, in concentrations ranging from 0% to 3%, is added into the mixture as an inhibitor to suppress explosions in the hydrogen-oxygen reaction system. Using detailed numerical simulations that include differential diffusion, thermal diffusion and additional modeling of surface reactions, the corresponding pressure-temperature explosion limits have been determined. Reaction pathway analysis shows that in general the chain-propagating step $HBr+H \rightarrow Br+H_2$ plays the most important role in consuming H radicals and slowing down the overall chemical reaction, effectively acting as a termination step. This explains the inhibitory effect of HBr in the hydrogen-oxygen reaction system. Importantly, the present work provides, for the first time, a unified analysis of how HBr modifies all three explosion limits and shows that HBr inhibition does not follow one universal mechanism. Instead, each explosion limit is governed by a different controlling reaction set, representing a new contribution beyond previous studies, which focused primarily on laminar flame inhibition or global suppression trends. More precisely, the three explosion limits are governed by different key reactions as follows:

- For the first explosion limit, even with the presence of HBr, the most important reactions are related to the consumption of H radicals by the chain branching reaction $H+O_2 \rightarrow OH+O$ and the chain termination reaction $H \xrightarrow{wall} \frac{1}{2}H_2$. Although the modeling of surface reactions involving reactive atomic Br is included, these surface reactions have almost no impact on the first explosion limit.
- For the second explosion limit, the most important reactions involve the competition between the chain branching step $H+O_2 \rightarrow OH+O$ and the chain termination step $H+O_2+M \rightarrow HO_2+M$. In the presence of HBr, the produced atomic Br is further consumed to form stable HBr molecules through two chain termination steps: $Br+HO_2 \rightarrow HBr+O_2$ and $Br+H+M \rightarrow HBr+M$. Therefore, the presence of HBr slows down the production rate of H radicals, thereby achieving the inhibitory effect.
- At even higher pressure at the third explosion limit, although the reaction $H+O_2+M \rightarrow HO_2+M$ still serves as a chain termination step, the produced HO_2 opens new reaction channels involving chain propagating steps such as $HO_2+HBr \rightarrow H_2O_2+Br$ and $HO_2+Br \rightarrow BrO+OH$. These reactions produce more reactive radicals than those on the reactant side; thus, while they are chain propagating steps, they have overall a promoting effect. Therefore, in the presence of HBr, the chain termination step $H+O_2+M \rightarrow HO_2+M$ has a negative sensitivity value of the explosion temperature with respect to its reaction rate, indicating its promoting effect on the explosion. The wall surface reaction $HO_2 \xrightarrow{wall} \frac{1}{2}H_2O+\frac{3}{4}O_2$ is important in the H_2-O_2 system but shows reduced sensitivity in the presence of HBr, as more HO_2 radicals participate in gas-phase reactions with Br-containing species.

The present study provides physical and chemical understanding on the inhibitory effect of HBr on explosion limits of stoichiometric hydrogen-oxygen mixture, offering practical insights into fire safety and explosion prevention in hydrogen-based industries. Finally, different hydrogen/oxygen chemical kinetics have been extensively discussed and compared in the literature, particularly with respect to ignition delay times and laminar flame speeds [45]. In contrast, the influence of different hydrogen/oxygen mechanisms on explosion limits has received less attention, and a systematic investigation of mechanism-dependent explosion-limit behavior is currently under preparation. Furthermore, because of the limited experimental data available for HBr-containing mixtures, the present model cannot be fully validated over the whole range of pressures and HBr concentrations examined. Therefore, the results should be viewed as providing qualitative mechanistic understanding. It is expected that future experimental studies will enable more comprehensive validation and refinement of the Br/H/O kinetic subset, thereby improving the predictive capability for inhibition phenomena involving bromine-containing species."

Acknowledgments

Authors thank Prof. Ulrich Maas for helpful discussion.

Open access funding enabled and organized by Projekt DEAL.

Conflicts of Interest

The authors declare no conflicts of interest.

Data Availability Statement

The data that support the findings of this study are available from the corresponding author upon reasonable request.

References

1. C. White, R. Steeper, and A. E. Lutz, "The Hydrogen-Fueled Internal Combustion Engine: A Technical Review," *International Journal of Hydrogen Energy* 31, no. 10 (2006): 1292–1305.

2. S. Verhelst and T. Wallner, "Hydrogen-Fueled Internal Combustion Engines," *Progress in Energy and Combustion Science* 35, no. 6 (2009): 490–527.

3. M. I. Shahid, A. Rao, M. Farhan, et al., "Hydrogen Production Techniques and Use of Hydrogen in Internal Combustion Engine: A Comprehensive Review," *Fuel* 378 (2024): 132769.

4. P. Lott, U. Wagner, T. Koch, and O. Deutschmann, "Hydrogen Combustion Engines–Chances and Challenges on the Way Towards a Decarbonized Mobility," *Chemie Ingenieur Technik* 94, no. 3 (2022): 217–229.

5. P. N. Rao, *Manufacturing Technology*, vol. 1 (Tata McGraw-Hill Education, 2013).

6. P. Marocco, M. Gandiglio, D. Audisio, and M. Santarelli, "Assessment of the Role of Hydrogen to Produce High-Temperature Heat in the Steel Industry," *Journal of Cleaner Production* 388 (2023): 135969.

7. K. Rechberger, A. Spanlang, A. Sasiain Conde, H. Wolfmeir, and C. Harris, "Green Hydrogen-Based Direct Reduction for Low-Carbon Steelmaking," *Steel Research International* 91, no. 11 (2020): 2000110.

8. Y. Qi, Y. Pan, S. Liu, J. Liu, R. Ye, and Z. Wang, "Explosion Hazards and Mechanisms of Hydrogen at Elevated Temperature and Pressure," *Journal of Loss Prevention in the Process Industries* 96 (2025): 105634.

9. V. Y. Plaksin and I. Kirillov, "Hydrogen Flammability and Explosion Concentration Limits for a Wide Temperature Range," *Journal of Loss Prevention in the Process Industries* 94 (2025): 105554.

10. D. A. Crowl and Y.-D. Jo, "The Hazards and Risks of Hydrogen," *Journal of Loss Prevention in the Process Industries* 20, no. 2 (2007): 158–164.

11. R. Ono, M. Nifuku, S. Fujiwara, S. Horiguchi, and T. Oda, "Minimum Ignition Energy of Hydrogen–Air Mixture: Effects of Humidity and Spark Duration," *Journal of electrostatics* 65, no. 2 (2007): 87–93.

12. E. Abohamzeh, F. Salehi, M. Sheikholeslami, R. Abbassi, and F. Khan, "Review of Hydrogen Safety During Storage, Transmission, and Applications Processes," *Journal of Loss Prevention in the Process Industries* 72 (2021): 104569.

13. H. D. Ng and J. H. Lee, "Comments on Explosion Problems for Hydrogen Safety," *Journal of Loss Prevention in the Process Industries* 21, no. 2 (2008): 136–146.

14. F. Yang, T. Wang, X. Deng, et al., "Review on Hydrogen Safety Issues: Incident Statistics, Hydrogen Diffusion, and Detonation Process," *International Journal of Hydrogen Energy* 46, no. 61 (2021): 31467–31488.

15. H. Liang, T. Wang, Z. Luo, et al., "Investigation on the Lower Flammability Limit and Critical Inhibition Concentration of Hydrogen Under the Influence of Inhibitors," *Fuel* 356 (2024): 129595.

16. H. Li, J. Li, W. Liang, and C. K. Law, "Role of Bromine Doping in Freely-Propagating Hydrogen-Oxygen Flames," *Proceedings of the Combustion Institute* 40, no. 1–4 (2024): 105257.

17. C. Hong, S. Xu, S. Zhao, et al., "Analysis of Ammonia as a Combustion Inhibitor for Combustion Knock and Power Expansion in a di Hydrogen Engine," *Fuel* 375 (2024): 132481.

18. D. Miller, R. Evers, and G. Skinner, "Effects of Various Inhibitors on Hydrogen-Air Flame Speeds," *Combustion and Flame* 7 (1963): 137–142.

19. M. van Wingerden, T. Skjold, D. Roosendans, A. Dutertre, and A. Pekalski, "Chemical Inhibition of Hydrogen-Air Explosions: Literature Review, Simulations and Experiments," *Process Safety and Environmental Protection* 176 (2023): 1120–1129.

20. V. I. Babushok, G. T. Linteris, D. R. Burgess Jr, and P. T. Baker, "Hydrocarbon Flame Inhibition by c3h2f3br (2-btp)," *Combustion and Flame* 162, no. 4 (2015): 1104–1112.

21. J. L. Pagliaro, N. Bouvet, and G. T. Linteris, "Premixed Flame Inhibition by cf3br and c3h2f3br (2-btp)," *Combustion and Flame* 169 (2016): 272–286.

22. B. A. Williams and J. W. Fleming, "Cf3br and Other Suppressants: Differences in Effects on Flame Structure," *Proceedings of the Combustion Institute* 29, no. 1 (2002): 345–351.

23. G. Dixon-Lewis, P. Marshall, B. Ruscic, et al., "Inhibition of Hydrogen Oxidation by hbr and br2," *Combustion and Flame* 159, no. 2 (2012): 528–540.

24. G. Von Elbe and B. Lewis, "Mechanism of the Thermal Reaction Between Hydrogen and Oxygen," *Journal of Chemical Physics* 10, no. 6 (1942): 366–393.

25. H. R. Heiple and B. Lewis, "The Reaction Between Hydrogen and Oxygen: Kinetics of the Third Explosion Limit," *Journal of Chemical Physics* 9, no. 8 (1941): 584–590.

26. D. Clark, R. Simmons, and D. Smith, "Inhibition of the Second Limit of the Hydrogen+ Oxygen Reaction by Hydrogen Bromide," *Transactions of the Faraday Society* 66 (1970): 1423–1435.

27. U. Maas and J. Warnatz, "Ignition Processes in Hydrogen-Oxygen Mixtures," *Combustion and Flame* 74, no. 1 (1988): 53–69.

28. J. Liu, J. Wang, N. Zhang, and H. Zhao, "On the Explosion Limit of syngas With co2 and h2o Additions," *International Journal of Hydrogen Energy* 43, no. 6 (2018): 3317–3329.

29. Z. Wang, X. Gou, and H. Zhang, "Explosion Limit of Hydrogen/Oxygen Mixture With Water Vapor Addition," *International Journal of Hydrogen Energy* 50 (2024): 772–781.

30. J. Li, W. Liang, W. Han, and C. K. Law, "On Explosion Limits of Hydrogen–Oxygen Mixtures With a Catalytic Platinum Surface," *Fuel* 391 (2025): 134773.

31. R. D. Richtmyer and E. Dill, "Difference Methods for Initial-Value Problems," *Physics Today* 12, no. 4 (1959): 50–50.

32. R. G. Hindman, "Generalized Coordinate Forms of Governing Fluid Equations and Associated Geometrically Induced Errors," *AIAA Journal* 20, no. 10 (1982): 1359–1367.

33. U. Maas, B. Raffel, J. Wolfrum, and J. Warnatz, "Observation and Simulation of Laser Induced Ignition Processes in o2- o3 and h2- o2 Mixtures," In *Symposium (International) on Combustion*, vol. 21, no. 1 (Elsevier, 1988), 1869–1876.

34. X. Wang and C. K. Law, "An Analysis of the Explosion Limits of Hydrogen-Oxygen Mixtures," *Journal of Chemical Physics* 138, no. 13 (2013): 742–751.

35. W. Liang and C. K. Law, "An Analysis of the Explosion Limits of Hydrogen/Oxygen Mixtures With Nonlinear Chain Reactions," *Physical Chemistry Chemical Physics* 20, no. 2 (2018): 742–751.

36. J. Li, W. Liang, J. Chen, W. Han, and C. K. Law, "Role of Surface Reactions in Hydrogen–Oxygen Explosion Limits," *Energy & Fuels* 36, no. 20 (2022): 12 729–12 736.

37. U. Maas and J. Warnatz, "Ignition Processes in Carbon-Monoxide-Hydrogen-Oxygen Mixtures," In *Symposium (International) on Combustion*, vol. 22, no. 1 (Elsevier, 1989), 1695–1704.

38. C. Yu, S. Eckart, S. Essmann, et al., "Investigation of Spark Ignition Processes of Laminar Strained Premixed Stoichiometric nh3-h2-Air Flames," *Journal of Loss Prevention in the Process Industries* 83 (2023): 105043.

39. S. Eckart, C. Yu, U. Maas, and H. Krause, "Experimental and Numerical Investigations on Extinction Strain Rates in Non-Premixed Counterflow Methane and Propane Flames in an Oxygen Reduced Environment," *Fuel* 298 (2021): 120781.

40. T. Noto, V. Babushok, A. Hamins, and W. Tsang, "Inhibition Effectiveness of Halogenated Compounds," *Combustion and Flame* 112, no. 1–2 (1998): 147–160.

41. C. N. Hinshelwood and E. Moelwyn-Hughes, "The Lower Pressure Limit in the Chain Reaction Between Hydrogen and Oxygen," *Proceedings of the Royal Society of London, Series A, Containing Papers of a Mathematical and Physical Character* 138, no. 835 (1932): 311–317.

42. M. Day, D. Stamp, K. Thompson, and G. Dixon-Lewis, "Inhibition of Hydrogen-Air and Hydrogen-Nitrous Oxide Flames by Halogen Compounds," In *Symposium (International) on Combustion*, vol. 13, no. 1 (Elsevier, 1971), 705–712.

43. D. Lee and S. Hochgreb, "Hydrogen Autoignition at Pressures Above the Second Explosion Limit (0.6–4.0 mpa)," *International Journal of Chemical Kinetics* 30, no. 6 (1998): 385–406.

44. S. R. Turns, *Introduction to Combustion*, vol. 287 (McGraw-Hill Companies New York, 1996).

45. C. Olm, I. G. Zsély, R. Pálvölgyi, et al., "Comparison of the Performance of Several Recent Hydrogen Combustion Mechanisms," *Combustion and Flame* 161, no. 9 (2014): 2219–2234.